A Molecular Dynamics Study on Heat and Mass Transfer in Condensation over Smooth/Rough Surface

Jie Sun, Ya-Ling He*, Wen-Quan Tao

State Key Laboratory of Multiphase Flow in Power Engineering, School of Energy and Power Engineering, Xi'an Jiaotong University, Xi'an, Shaanxi, 710049, P.R.China

Abstract:

Purpose –The paper focuses on the condensation process of hot vapor on smooth/rough walls and aims to find how the condensation film forms and grows. The influences of the roughness and the wettability on condensation are especially analyzed.

Design/methodology/approach –The non-equilibrium molecular dynamics simulation method is used to simulate the condensation. In order to maintain the process, a simple and effective molecule insertion mechanics is proposed.

Findings –The results show that the wall-neighboring liquid structure becomes more regular with stronger wettability. The temporal parametric profiles show that the condensation doesn't progress at a constant rate but exhibit obvious unsteady characteristics of gradual deceleration, especially for strong wettability cases. Analysis based on heat and mass transfer indicates that the influence of wettability is quite superior to that of the roughness. The enhancement should be explained by the more fluent and effective energy exchange between solid and liquid particles caused by strong solid-liquid coupling other than by the ordering structure itself.

Practical implications –Our findings have provided the suggestion that the wettability should be paid on special attention when the heat transfer performance of the microscale condensation is predominantly focused on.

Originality/value –The paper provides a vapor-liquid-solid model with molecule insertion. This model can be used to evaluate the contact thermal resistance and the thermal boundary conditions in condensation under different geometric conditions.

Keyword: Non-equilibrium molecular dynamics; Condensation; Wettability; Interface; Temperature jump;

The Kapitza resistance

* Corresponding author, E-mail: yalinghe@mail.xjtu.edu.cn

A Molecular Dynamics Study on Heat and Mass Transfer in Condensation over Smooth/Rough Surface

Jie Sun, Ya-Ling He*, Wen-Quan Tao

State Key Laboratory of Multiphase Flow in Power Engineering, School of Energy and Power Engineering, Xi'an Jiaotong University, Xi'an, Shaanxi, 710049, P.R.China

Abstract:

Purpose –The paper focuses on the condensation process of hot vapor on smooth/rough walls and aims to find how the condensation film forms and grows. The influences of the roughness and the wettability on condensation are especially analyzed.

Design/methodology/approach –The non-equilibrium molecular dynamics simulation method is used to simulate the condensation. In order to maintain the process, a simple and effective molecule insertion mechanics is proposed.

Findings –The results show that the wall-neighboring liquid structure becomes more regular with stronger wettability. The temporal parametric profiles show that the condensation doesn't progress at a constant rate but exhibit obvious unsteady characteristics of gradual deceleration, especially for strong wettability cases. Analysis based on heat and mass transfer indicates that the influence of wettability is quite superior to that of the roughness. The enhancement should be explained by the more fluent and effective energy exchange between solid and liquid particles caused by strong solid-liquid coupling other than by the ordering structure itself.

Practical implications –Our findings have provided the suggestion that the wettability should be paid on special attention when the heat transfer performance of the microscale condensation is predominantly focused on.

Originality/value –The paper provides a vapor-liquid-solid model with molecule insertion. This model can be used to evaluate the contact thermal resistance and the thermal boundary conditions in condensation under different geometric conditions.

Keyword: Non-equilibrium molecular dynamics; Condensation; Wettability; Interface; Temperature jump;

The Kapitza resistance

* Corresponding author, E-mail: yalinghe@mail.xjtu.edu.cn

Nomenclature

A	transverse section area. nm^2
A_c	solid-liquid contact area. nm^2
d	distance. nm
D	the distance between two convexities. nm
e	specific internal energy. kJ/kg
$\mathbf{f}$	interaction force vector. N
$\mathbf{F}$	random force vector. N
H	the height of the convexity. nm
h	specific enthalpy. kJ/kg
k	spring constant. N/m heat transfer coefficient. $MW/(m^2 \cdot K)$
k_B	Boltzmann constant. J/K
L	length. nm
m	mass of particle. kg
$\dot{m}$	mass flux. $kg/(s \cdot m^2)$
N	number of meshes, number of molecules, count of loops
N'	number of molecules in condensation period
ΔN	number of molecules with those velocities between v and $v+\Delta v$
n	integral part
O	geometrical center. nm
p	pressure. MPa
$\mathbf{p}$	momentum vector. $kg \cdot m/s$
q	heat flux. MW/m^2
R	random point. nm the Kapitza resistance. $m^2 \cdot K/W$
r	distance. nm
r_c	cut-off radius. nm
T	temperature. K
T_j	temperature jump. K
$T_{j,D}$	the temperature jump at the bottom surface. K
$T_{j,W}$	the temperature jump at the top surface. K
$\overline{T}_{j,H}$	the mean temperature jump at the lateral surface. K
T_H	high temperature. K
T_L	low temperature. K
t	time. ns
t'	time in condensation period. ns
t_0	the starting time of condensation period. ns
δt	time step of simulation. fs
u	potential energy. J
Δu	potential energy drop. kJ/kg
v	velocity. m/s
v_m	most probable velocity. m/s

Δv	the increment of velocity. m/s
W	the width of the convexity. nm
x,y,z	dimension. nm

Greek symbols

α	damper constant. 1/s
β	adjusting factor for wettability
γ	latent heat. kJ/kg
ε	characteristic energy. J
λ	thermal conductivity. $\mathrm{W/m \cdot K}$
ρ	density. $\mathrm{kg/m^3}$
σ	characteristic length. nm

Subscript

0	related to equilibrium period
1,2,3,4	index
Ar	argon
Ar-Ar	related to an argon-argon pair
Ar-Pt	related to an argon-platinum pair
c	condensation
e	experimental data
F	random force
in	inlet
I	the ith
l	liquid
lh	latent heat
out	outlet
set	preset value
sh	sensible heat
v	vapor
w	solid wall
x,y,z	dimension

1. Introduction

The phenomenon of condensation is of great fundamental importance for various fields of science and engineering. Although this phase-change process has been studied both theoretically and experimentally (Penner, 1952; Wegener and Pouring, 1964; Cammenga, 1980), there still exist problems and the unknown causes seem to be under discussion now. In order to solve the problems and to have a better understanding of the condensation process in microscale, a new researching method is badly needed. It is known that a series of theoretical/numerical methods were established on the basis of classical continuum medium model, which will become invalid at molecular level and it is still difficult to take experimental research under such small temporal (picosecond) and spatial (nanometer) scales. The classical molecular dynamics simulation (MDS), which is a particle-focused computer-aided method, has shown its ability to describe the N-body problem and has been proven quite promising for the exploration to the microscopic world.

The liquid-vapor interface under equilibrium condition has been widely studied with equilibrium

molecular dynamics simulation (EMDS). Matsumoto and his co-workers (1994; 1994; 1995; 1996) divided the interfacial molecular behaviors into four types and proved that the fourth type, i.e. “molecular exchange” behavior, is significant to the condensation of associating fluids and fluids at high temperature. Meland (2002) studied molecular exchange mechanism and its influence on the condensation coefficient. Yang and Pan (2005) revealed the four types of molecular behaviors mentioned above in their water system and showed that the hydrogen bond has a significant influence on the molecular behaviors and may reduce the evaporation coefficient. Tsuruta et al. (1999) found that the condensation/evaporation coefficients depend on the surface-normal component of translational energy. The vapor molecules with smaller energy can be easily reflected by the surface molecules, and the surface molecules with smaller energy can not evaporate. Nagayama and Tsuruta (2002; 2003) conducted researches of interfacial mass transfer based on the transition-state theory and an evaluation of the transition state was considered by applying the results of MD simulation for argon and water cases.

In retrospect to the open publications, the equilibrium system of liquid-vapor interface is often used to study the properties such as the condensation/evaporation coefficients, surface tensions, and so on. However, the condensation/evaporation processes in practical engineering applications often occur under obvious non-equilibrium conditions with overheating or overcooling states, for example the hot vapor condenses on a cool surface and the condensation film or droplet is heated and vaporized. It has been found that these phase-change processes behave quite differently under equilibrium and non-equilibrium conditions, which indicate that the condensation/evaporation coefficients are strongly influenced by the ambient conditions (Matsumoto and Fujikawa, 1997). These kinds of phenomena are commonly seen in the engineering fields relevant to heat and mass transfer, thus they should be paid on more attention. A brief review will be provided as follows.

A numerical experiment using non-equilibrium molecular dynamics simulation (NEMDS) method was carried out by Maruyama and Kimura (1999b) and it was found that the contact thermal resistance, i.e. the Kapitza resistance, over the liquid-solid interface is caused by a distinctive jump in the temperature distribution in the normal direction. The resistance, which had strong dependence on the wettability, was 5-20nm thickness of liquid heat conduction layer. Yi et al. (2002) simulated the vaporization of an ultra-thin liquid layer on a solid surface with a solid-liquid-vapor system and showed the Leidenfrost phenomenon during the process in high surface temperature case. Meland et al. (2004) studied the net condensation/evaporation process with a modified model originated from the equilibrium liquid-vapor one. The interfacial thermal resistance was studied by Wang et al. (2007) in a nano-triangular channel and the understanding was gained that the overall thermal resistances are determined by the balance of two parts: the thermal resistance at the solid-liquid interface and that attributed to vapor adsorption on the lateral surface. In addition, the interfacial phenomena such as droplet evaporation, bubble nucleation and droplet spreading on solid surface have also interested researchers (Maruyama and Kimura, 1999a; Maruyama, 2000; Maruyama *et al.*, 2002; Consolini *et al.*, 2003; Poulikakos *et al.*, 2003; Nagayama *et al.*, 2006). Although there have been already some simulation results showing accordance with experimental data qualitatively or quantitatively, the non-equilibrium processes still need more effort to be made on for promotion in practical application.

It is well known that the phase-change heat-exchangers often have better performances than the ordinary ones because of the existence of latent heat. Condensation is usually divided into two types: dropwise or filmwise. Since the latent heat released by the vapor has to be transferred through the condensate film where the resistance exists, it is obvious that the former type is superior to the latter in performance. Based on this understanding, the latter type, which is more common in industry, is often

optimized with the guideline of destroying or reducing the condensate film. Therefore, a primary and essential job is to explore how the film forms and grows over the solid surface, where the microscopic roughness should also be taken in consideration because it can never be avoided during practical machining. It has been found that the micro-structure has shown significant influence on the microchannel fluid flow (Cao *et al.*, 2006a; b; Ziarani and Mohamad, 2008), but the reports on its influence in the heat transfer of phase-change process are seldom seen. To study this issue, the previous models (Maruyama and Kimura, 1999b; Yi *et al.*, 2002) are improved and a simple molecule insertion mechanics is presented in order to maintain the unsteady condensation for a comparatively long time. With insertion, the phenomenon of hot vapor condensing on a smooth/rough solid wall is successfully simulated. The influence of vapor-solid temperature difference, liquid-solid bonding and surface roughness on the heat and mass transfer characteristic are specially focused on. The present work can be considered as a microscopic model ready to provide thermal boundary conditions for filmwise condensation under different types of solid surfaces.

2. Molecular dynamics simulation

2.1 Computational model

The simulation box is a cuboid of $L_x \times L_y \times L_z = 4.94\text{nm} \times 3.30\text{nm} \times 39.54\text{nm}$, where $L_x : L_y : L_z \approx 3:2:24$ and L_i is the length in i direction. Large ratios between vertical and horizontal directions are chosen in order to avoid the condensation at the bottom being affected. The origin is set at the geometric center. The solid wall is set at the bottom with either smooth surface (SS) or rough surface (RS) comprised of periodic rectangular concavo-convex. Periodic boundary conditions are used in *x*- and *y*- directions, and the mirror boundary condition is used at the top throughout the simulations. Fig. 1 shows the configuration of the system.

Argon molecules are initially arranged in face-centered cubic (FCC) pattern in the cuboid with the saturated density corresponding to the high temperature $T_{\mathrm{H}}(=T_{\mathrm{v}})$. The initial 0.1ns ($t_0$) is called the equilibrium period, which is used to allow the system reach its thermal equilibrium state at T_{H}. The mechanics known as Gauss's principle of least constraint (Rapaport, 2004) and the 'phantom method' (Blomer and Beylich, 1999) are employed to keep the vapor and the solid at preset temperatures, respectively. Immediately after that, the wall temperature is shifted to a low value of $T_{\mathrm{L}}(=T_{\mathrm{w}})$ and the condensation period begins. This period lasts for 10ns with the time step $\delta t \approx 5\text{fs}$. While the condensation is proceeding, the vapor will become less and less. Therefore, extra vapor molecules need to be inserted into the system with a set of mechanics and the temperature and density in the insertion region are kept constant so that the condensation could be kept in progress as if the cuboid was connected with a large vapor bulk. In order to obtain the parametric profiles by statistical averaging every 0.1ns, the cuboid is divided equally in *x*- and *z*- directions by a uniform mesh of $N_x \times N_z = 150 \times 360$.

The modified Lennard-Jones (L-J) potential is used for an argon-argon pair (Ar-Ar):

$$\begin{aligned} u(r) = 4\varepsilon_{\text{Ar-Ar}} \Big\{ \Big[(\sigma_{\text{Ar-Ar}}/r)^{12} - (\sigma_{\text{Ar-Ar}}/r)^{6} \Big] + \Big[6(\sigma_{\text{Ar-Ar}}/r_{\mathrm{c}})^{12} - 3(\sigma_{\text{Ar-Ar}}/r_{\mathrm{c}})^{6} \Big] (r/r_{\mathrm{c}})^2 \\ - 7(\sigma_{\text{Ar-Ar}}/r_{\mathrm{c}})^{12} + 4(\sigma_{\text{Ar-Ar}}/r_{\mathrm{c}})^{6} \Big\} \end{aligned} \tag{1}$$

where $\sigma_{\text{Ar-Ar}} = 0.341\text{nm}$ and $\varepsilon_{\text{Ar-Ar}} = 1.67 \times 10^{-21}\text{J}$ are the length and energy characteristic parameters, respectively. The cutoff radius is set as $r_{\mathrm{c}} = 3.5\sigma_{\text{Ar-Ar}}$. Stoddard and Ford (1973) recommended this function based on the fact that when r increases to r_{c}, both u and $\mathrm{d}u/\mathrm{d}r$ go continuously to zero

and no discontinuous forces will appear.

The interaction between an argon-platinum pair (Ar-Pt) is also governed by Eq.(1) but the characteristic parameters are changed into $\sigma_{\text{Ar-Pt}} = 0.309\text{nm}$ and $\varepsilon_{\text{Ar-Pt}} = 0.894\times10^{-21}\text{J}$ (Yi *et al.*, 2002). Besides, a factor β from 0.4 to 1.6 is added before $\varepsilon_{\text{Ar-Pt}}$, through which the wettability of the wall can be adjusted from weak to strong correspondingly.

2.2 Solid wall at constant temperature

In order to keep the solid wall at a target temperature T_{w}, the 'phantom method' (Blomer and Beylich, 1999; Maruyama and Kimura, 1999a; b; Maruyama, 2000; Yi *et al.*, 2002) is employed because it is less artificial compared with simple velocity rescaling. Three layers of Pt atoms are arranged in FCC (111) structure called the 'real' atoms with the atomic mass $m_{\text{Pt}} = 3.24\times10^{-25}\text{kg}$, the neighboring distance $\sigma_{\text{Pt}} = 0.277\text{nm}$ and the spring constant $k = 46.8\text{N/m}$ (Maruyama and Kimura, 1999b; Yi *et al.*, 2002). To model the semi-infinite solid wall, another two layers of 'phantom' atoms are arranged right below the real ones with the lower layer fixed as a frame. A special spring of $2k$ in vertical and $0.5k$ in horizontal directions is applied to represent the harmonic interaction between a real atom and the phantom one below it. Similarly, a special spring of $2k$ in vertical and $3.5k$ in horizontal directions is applied to represent the harmonic interaction between a phantom atom and the phantom one below it. The configuration is shown in Fig. 2.

The phantom atoms in the upper layer are controlled by the 3D Langevin equation:

$$\frac{\mathrm{d}\mathbf{p}_i(t)}{\mathrm{d}t} = -\alpha\mathbf{p}_i(t) + \mathbf{f}(t) + \mathbf{F}(t) \tag{2}$$

where $\alpha = 1.61\times10^{13}/\text{s}$ is the damper constant (Yi *et al.*, 2002); $\mathbf{p}_i(t)$ is the momentum vector of *i*th phantom atom; $\mathbf{f}_i(t)$ is the interaction force vector between *i*th phantom atom and its neighbors; $\mathbf{F}_i(t)$ is the random exciting force vector, of which the components are sampled independently at each time step from a Gaussian distribution with zero mean value and standard deviation $\sqrt{2\alpha k_{\text{B}}T_{\text{w}}/\delta t}$ (k_{B} is the Boltzmann constant). With this method, the wall temperature T_{w} can be well controlled constant at a target value.

2.3 Molecule insertion

The condensation will cause a gradual density decrease in the vapor bulk, which can finally lead the system to a steady state if N_{Ar} is constant. On the one hand, our main attention is focused on the condensate film formed over the wall. The growth is expected to be kept for a period as long as possible, which means a large N_{Ar} is needed. On the other hand, the condensation only occurs at the liquid-vapor interface in the vicinity of the wall. Apparently, it is computationally expensive if the vapor molecules distant from the wall are considered. Therefore, inserting vapor molecules whenever needed is an economic way of solving the contradiction. The insertion is carried out in a simple way based on Meland's idea (2004). He has presented a method of extracting vapor molecules and inserting them into the liquid bulk to keep the steady-state evaporation. In his statement, the molecules are simply inserted in the center of a triangle formed by one molecule and its two nearest neighbors. Since finding the three molecules costs no more than finding the four nearest to a certain point, it is more reasonable to insert a molecule in the center of a tetrahedron rather than a triangle for a three-dimensional simulation. Besides,

if the three molecules are so near to each other, the unphysical repulsive forces would become extremely large and could probably cause errors, therefore some adjustments should be adopted afterwards. With the considerations mentioned above, a simple method is proposed as follows with flow chart and schematic shown in Fig. 3:

1. judge whether the vapor density in the insertion region decreases, if yes, continue with step 2; if not, jump to step 7;
2. generate a random point (R) with uniform distribution in the insertion region;
3. find the four nearest molecules ($m_1 \sim m_4$) to the point R, calculate the coordinates of the geometrical center (O) of the tetrahedron formed by the four molecules and the distances ($d_1 \sim d_4$) between the molecules and the center;
4. if the minimum of d_i ($i = 1 \sim 4$) is larger than d_{set}, continue with step 5; if not, jump to step 6;
5. insert the molecule at O, jump to step 7;
6. if the minimum of d_1 ($i = 1 \sim 4$) is smaller than d_{set} but N is also smaller than 500, reset $d_{\text{set}} = 0.95^n d_{\text{v}}$ and jump back to step 2; if N is larger than 500, jump to step 7;
7. quit the subroutine.

The insertion region is of $L_z / 10$ thick at the top (see Fig. 1). N is the count of loops of step 2~4 and 6. n is the integral part of $N/100$. d_{v} is the average intermolecular distance according to the vapor density. d_{set} is the threshold length, which is set equal to d_{v} for the first loop and will decrease gradually when the random point is not suitably generated. The mechanics can make it easier to find an available point before the limitation of $0.98^5 d_{\text{v}} \approx 0.90 d_{\text{v}}$ is reached. There are two exits for the subroutine, namely completion and abortion. The loop limitation of 500 can avoid the subroutine from generating random points all the time. The whole mechanics can provide a comparatively suitable position where even the minimum intermolecular distance is still larger than d_{set}. In practical applications, N seldom gets larger than 400 (mean value 135), which means the preset constants are suitable and the insertion completes almost each time when executed.

In addition, the velocity components of each vapor molecule inserted are sampled from a Gaussian distribution in order to reasonably keep the average temperature equal to T_{H}. Some rescaling adjustment is carried out immediately after the insertion, if necessary, to avoid physically unrealistic huge velocities.

2.4 Definitions of bulk regions and molecular states

In our simulations, the liquid-vapor interface is shifting gradually with the condensation process. The positions where the interface region starts and ends should be clearly defined. The simple method based on the intermolecular distance and the complicated definition method SRK criterion with consideration of the state equations (Meland *et al.*, 2004) are both preconsidered. It has been found that the deviation between the two methods is neglectable if the coefficients are carefully chosen by trial and error, especially for the low temperature cases. Therefore the former is employed in the present work for its simplicity. $1.04d_1$ and $2.15d_1$ are used to define a molecule as liquid, vapor or an intermediate molecule. A molecule is defined as a liquid molecule if the distance between it and a liquid one is smaller than $1.04d_1$, or an intermediate molecule if the distance is between $1.04d_1 \sim 2.15d_1$, or a vapor molecule if the distance is larger than $2.15d_1$. Here, the values of $1.04d_1$ and $2.15d_1$ correspond to 90% and 10% of fluctuation ρ_1, which are chosen as thresholds by trial and error. The liquid molecules nearest to the solid wall should be confirmed at initial. In practical application, average values over 500 ps are used to check the states instead of instant values.

3. Results and discussion

Simulation conditions are shown in Table 1. The smooth case labeled S2 is firstly carried out to study how the parameters vary and how the condensate film grows during the condensation process. Then, the influences of different T_H and β on the heat and mass transfer are investigated. After that, RS cases are carried out similarly. For convenience, we use N'_{Ar} and t' to indicate $N_{Ar} - N_{Ar,0}$ and $t - t_0$ from then on.

3.1 Smooth surface cases

The system reaches its vapor-solid thermal equilibrium state after the initial 0.1ns when the temperature, pressure and density show uniform. The molecular velocities are in accordance with the Maxwellian distribution (see Fig. 4).

Fig. 5 shows few layers of vapor molecules are absorbed by the solid atoms before $t' = 0$, which form an ultra thin film. As vapor molecules condense after $t' = 0$, the film grows thicker and the liquid molecules adjacent to the wall gradually arrange in an ordered layering pattern showing density oscillation, of which the amplitude decreases with increasing distance. This phenomenon is called 'liquid layering', which has been widely studied by numerical and experimental methods (Forcada and Mate, 1993; Huisman *et al.*, 1997; Maruyama and Kimura, 1999b; Xue *et al.*, 2003; Nagayama and Cheng, 2004; Xue *et al.*, 2004). It has been found that the oscillatory magnitude and range increase with increasing solid-liquid coupling strength, i.e. wettability, which has closely relationship with the flow and thermal slip boundaries. The layering range is usually of only several molecular diameters. For S2 case, the average liquid density is $1.196\times10^3\,\mathrm{kg/m^3}$, so the volume occupied by one molecule is $0.0560\mathrm{nm}^3$ with the molecular mass $m_{Ar} = 6.69\times10^{-26}\,\mathrm{kg}$. Therefore, the thickness of one layer should be $0.383\mathrm{nm}$. Fig. 5 shows that the oscillation range is about $2.351\mathrm{nm}$ thick with 6 peaks, i.e. $0.392\mathrm{nm}$ per layer, which indicates a regular structure with one layer closely adjacent to another in the condensate film. The local radius distribution function obtained in the wall-neighboring region (see Fig. 7) also illustrates this regular structure.

The local temperature near the wall drops and a temperature gradient forms in *z*-direction in the condensate film gradually after $t' = 0$, until a comparatively steady state is reached. The upper panel of Fig. 6 shows that the temperature gradient is $\partial T / \partial z = 1.125\mathrm{K/nm}$ and the temperature jump is $T_j = 5.30\mathrm{K}$, which agrees with the value of 5.90K from Maruyama and Kimura (1999b) under the similar conditions. It also can be seen that a potential drop appears near the wall and the range gets wider (see the middle panel of Fig. 6). The potential energy drop Δu is defined as the difference between the average values in the vapor and liquid bulks, and it is about $105.2\mathrm{kJ/kg}$ for S2 case.

The molecule number increases comparatively intensively before $t' = 3\mathrm{ns}$ and then increases basically linearly (see Fig. 8). The molecule insertion is carried out along with the condensation process. The initial velocity components and kinetic temperature of each inserted molecule have been recorded. Fig. 9 shows that the distribution of the velocity components agrees well with the Gaussian distribution with zero mean value and standard deviation $\sigma = \sqrt{k_B T_v / m_{Ar}}$. Besides, Figs. 5~6 have shown uniform parametric profiles in the vapor bulk without unphysical fluctuations, which have proved the reliability and stability of the insertion mechanics.

In order to analyze the heat and mass transfer characteristics in the simulation system, the rate form of the general energy balance is used according to the first law of thermodynamics (Cengel and Boles, 2002):

$$\Delta \dot{e} = \dot{e}_{\text{in}} - \dot{e}_{\text{out}} \tag{3}$$

where $\Delta \dot{e}$ is the rate of change in specific internal energy in the system, which corresponds to the latent heat γ; $\dot{e}_{\text{in}}$ and $\dot{e}_{\text{out}}$ are the rate of net energy transfer in and out of the system, which correspond to the heat transfer in the vapor inflow and the thermal conduction in the condensate film. Therefore, Eq.(3) can be further written as:

$$\dot{e}_{\text{out}} = \dot{e}_{\text{in}} - \Delta \dot{e} = q_{\text{v}} - \left(-\gamma \dot{m}_{\text{c}}\right) \tag{4}$$

where q_{v} is the heat fluxes in vapor region; $\dot{m}_{\text{c}}$ is the condensation mass flux. It can be clearly seen that the first and second terms correspond to the sensible ($q_{\text{sh}} = q_{\text{v}}$) and latent ($q_{\text{lh}} = \gamma \dot{m}_{\text{c}}$) parts of the heat transferred through the condensate film ($q_{\text{l}} = \dot{e}_{\text{out}}$). Note that the negative sign in the second term means the energy is released from the system. In practical simulation of S2 case, $q_{\text{v}} = 40.46\text{MW/m}^2$ is directly calculated statistically within $t' = 8 \sim 10\text{ns}$, which is a comparatively steady condensation period, according to Maruyama (2000):

$$q_{\text{v}} = \frac{1}{2V}\left[\sum_i m_{\text{Ar}} v_i^2 v_{i,z} + \sum_i \sum_{j \neq i} u(r_{ij}) v_{i,z} - \sum_i \sum_{j \neq i} \left(\mathbf{r}_{ij} \mathbf{f}_{ij}\right) v_{i,z}\right] \tag{5}$$

where the first and second terms are related to summations of kinetic and potential energy carried by *i*th molecule; the third term represents the energy transfer by the pressure work; V is the volume of vapor bulk. $\dot{m}_{\text{c}}$ can be obtained by calculating the variation rate of N_{Ar}:

$$\dot{m}_{\text{c}} = \frac{m_{\text{Ar}}}{A}\left(\frac{\text{d}N_{\text{Ar}}}{\text{d}t}\right) \tag{6}$$

where A is the transverse section area. For S2 case, $\dot{m}_{\text{c}}$ is calculated to be $526.9\text{kg/s}\cdot\text{m}^2$ by linearly fitting the corresponding data within $t' = 8 \sim 10\text{ns}$ in Fig. 8. γ is in principle the difference between the enthalpies of vapor and liquid at saturated state (Cengel and Boles, 2002):

$$\gamma = \Delta h_{\text{s}} = h_{\text{s,v}} - h_{\text{s,l}} \tag{7}$$

where $h = e + p/\rho$ contains the internal energy including kinetic and potential energies, and the pressure work. The enthalpy profile averaged between $t' = 8 \sim 10\text{ns}$ is shown in the lower panel of Fig. 6, from which γ is determined to be 122.3kJ/kg for S2 case. This predicted value agrees well with the experimental value 123.7kJ/kg (NIST, 2005) corresponding to the saturated temperature 122K. Therefore, the heat flux can be calculated as $q_{\text{l}} = 104.9\text{MW/m}^2$ according to Eq.(4). The thermal conductivity λ is then calculated as $\lambda = q_{\text{l}} / (\partial T / \partial z) = 0.093\text{W/m}\cdot\text{K}$ based on the Fourier's law. The predicted value lies just in the experimental range of $0.102 \sim 0.095\text{W/m}\cdot\text{K}$ (NIST, 2005) corresponding to the temperature range of $105 \sim 111\text{K}$ in the condensate film. Further, the Kapitza resistance R and the heat transfer coefficient k can be predicted as $R = T_{\text{j}} / q_{\text{l}} = 0.051 \times 10^{-6}\,\text{m}^2\cdot\text{K/W}$.

Similar simulations and analysis under different vapor temperature ($T_{\text{v}} = 110 \sim 130\text{K}$) are carried out sequentially. The simulation conditions and results are listed in Table 1 and 2. The results agree with the

experimental values (NIST, 2005) and thus validate our codes. It is found that the condensation mass flux $\dot{m}_c$ increases obviously with increasing T_v, which means the mass transfer is intenser. When we focus on the heat transfer, it is found that both the latent heat flux q_{lh} and the sensible heat flux q_{sh} increases with increasing T_v. Although γ becomes lower, the great increase in $\dot{m}_c$ ensures q_{lh} is still increasing. In addition, the results also show that the ratio of q_v / q_l also decreases obviously, which means the latent heat part is becoming predominant in the overall heat flux with increasing T_v.

The influence of wettability for SS cases is studied with $T_v = 120\text{K}$ and $\beta = 0.4 \sim 1.4$, which are listed in Table 1 as S4~S8 cases. The temporal variation of N'_{Ar} is shown in Fig. 8, from which we can find that $\dot{m}_c$ increases with increasing β but decreases with time especially for large β, which means that the mass transfer decelerates gradually during the condensation process especially for high wettability case. The temporal heat flux q_l and the ratios of q_{lh} / q_l and q_{sh} / q_l are shown in Fig. 10. By comparing Fig. 10 with Fig. 8, the unsteady characteristic can be clearly seen that q_l is large at initial because of large $\dot{m}_c$ and then gradually decreases with decreasing $\dot{m}_c$. During this variation, the ratio of q_{lh} / q_l almost keeps constant around 0.6. It is worth mentioning that the ratio of q_{lh} / q_l for the very weak wettability case (S4) shows a remarkable decrease with time. The local radius distribution functions in Fig. 7 shows that the weaker or stronger wettability corresponds to the less or more regular wall-neighboring liquid structure, further showing the weaker or stronger coupling between solid and liquid particles. The above results may indicate that when the liquid is very non-wetting, the heat transfer is weakened and the sensible heat takes up the predominant part, because the liquid-solid coupling is so weak that the energy transfer across the interface is greatly baffled. The temporal values of T_j and R provide a good proof for what is mentioned above (see Fig. 11). Besides, by comparing the results of S3 with S7~S8, it is indicated that if the wall is well wetting, the heat transfer performance can be kept even equivalent though T_v is lowered.

The heat and mass transfer variation has shown that the condensation doesn't progress at a constant rate but exhibits obvious unsteady characteristics especially for large β cases. It can be concluded that the process accelerates at initial and gradually decelerates afterwards, which agrees with the macroscopic regularity. The heat and mass transfer is strengthened with increasing β, because stronger liquid-solid bonding makes R smaller and further makes the transfer across the liquid-solid interface more fluently.

3.2 Rough surface cases

The two-dimensional density profiles of R7, R3 and R8 cases are illustrated in Fig. 12, from which a meshy distribution can be clearly seen in the concave region with staggered local maximum and minimum and the magnitude increases with increasing β. The different wall-neighboring liquid structures caused by the different wettabilities can also be clearly seen from the systematic snapshots in Fig. 12, where the layering and meshy region is larger and more obvious with increasing β. This regular structure can be comprehended as the synthesis of the *x*- and *z*- layerings (see Fig. 13).

Fig. 12(e) and Fig. 13 show that obvious temperature gradient only exists in *z*-direction in the liquid bulk. It is found that T_j in the concave is smaller than that on the convexity or in SS cases with the same wall temperature because of the action of the lateral surfaces. In order to calculate the Kapitza resistance and compare with SS cases conveniently, we define an area-weighted average T_j for RS cases as:

$$T_j = \left(W \cdot T_{j,W} + 2H \cdot \overline{T}_{j,H} + 2D \cdot T_{j,D} \right) / \left(W + 2H + 2D \right) \tag{8}$$

where $T_{j,W}$ and $T_{j,D}$ are the temperature jumps at the top and the bottom surfaces, $\overline{T}_{j,H}$ is the linear averaged T_j at the lateral surface.

Fig. 14 and Fig. 15 show that the mass and heat transfer is strengthened with increasing H. It is commonsense that larger contact area (A_c) can enhance the heat transfer further the mass transfer, but its effect seems quite inferior to wettability. Comparatively speaking, increasing the collision chance between solid and liquid particles is far less advisable than improving the collision effect of a solid-liquid pair for the enhancement in heat transfer. The results also indicate that when both H and β are increased, the effect will be greatly improved mainly because more liquid molecules can effectively exchange their energy with solid atoms with smaller resistance, as shown in Fig. 16.

A more intuitive comparison of average heat flux ($\overline{q}$) during $t' = 2\text{ns}\sim10\text{ns}$ is provided in Fig. 17, where the result of S2 case is set as the benchmark and the results of other cases are compared in the increment ratios. It is easy to find out that the variation of $\overline{q}$ is more sensitive to β than to A_c. For example, S8 and R1 cases are specially chosen with similar magnitude of increment ratios in β (40%) and A_c (37%) but the corresponding increment ratios of $\overline{q}$, i.e. 58% and 20%, are quite different. This quantitative comparison reveals that the wettability (β) has much stronger influence on the heat transfer in condensation compared to the roughness induced contact area (A_c). However, the heat transfer enhancement caused by increasing β becomes smaller when $\beta = 1.4$, which probably indicates that the enhancement by β is limited. After all, the largest heat transfer enhancement is obtained by increasing both β and A_c.

4. Conclusions

In the present paper, the condensation processes of argon vapor over smooth/rough platinum surfaces were simulated with NEMD method. The following conclusions have been drawn:

(1) A simple and effective molecule insertion mechanics was proposed as a steady vapor supply source to maintain the condensation process. The code is primarily validated by the experimental data.

(2) The wall-neighboring liquid structure shows more regular with increasing β by the radius distribution functions. The temporal profiles have quantitatively shown that the condensation doesn't progress with a constant rate but exhibit obvious unsteady characteristic with acceleration for an initial period and gradual deceleration afterwards, especially for large β cases. This characteristic agrees with the macroscale commonsense that with the growth of the condensate film, the interfacial resistance increases leading the condensation to decelerate until a steady state is finally reached.

(3) By comparing the simulation results, we can find that the mass and heat transfer can be enhanced with increasing A_c or β or both, but the influence of β is quite superior to that of A_c. It can be explained by more fluent and effective energy exchange between solid and liquid particles caused by larger β, which has been proved by the results in the present work and those in Maruyama and Kimura's work (1999b). The present results indicate that the wettability, which is often negligible in macroscale, should be considered as a predominant factor of heat transfer enhancement in condensation for those who focus on micro-/nano-scale thermal engineering, because in such small scales the interfacial interaction always plays a very important role.

Further study should be carried out to obtain the thermal boundary conditions for condensation under different kinds of surfaces. Those boundary conditions can be used for the macroscopic methods such as finite volume/element method dealing with condensation process.

Acknowledgements

The present work was supported by the National Natural Science Foundation of China (No. U0934005, 50636050).

References

Blomer, J. and Beylich, A.E. (1999), "Molecular dynamics simulation of energy accommodation of internal and translational degrees of freedom at gas-surface interfaces", *Surf. Sci.*, Vol. 423 No. 1, pp. 127-33.

Cammenga, H.K. (1980) *Evaporation mechanisms of liquids*, North-Holland, Amsterdam.

Cao, B.Y., Chen, M. and Guo, Z.Y. (2006a), "Effect of surface roughness on gas flow in microchannels by molecular dynamics simulation", *Int. J. Eng Sci*, Vol. 44 No. 13-14, pp. 927-37.

Cao, B.Y., Chen, M. and Guo, Z.Y. (2006b), "Liquid flow in surface-nanostructured channels studied by molecular dynamics simulation", *Phys. Rev. E*, Vol. 74 pp. 066311.

Cengel, Y.A. and Boles, M.A. (2002) *Thermodynamics: An engineering approach*, McGraw-Hill, New York.

Consolini, L., Aggarwal, S.K. and Murad, S. (2003), "A molecular dynamics simulation of droplet evaporation", *Int. J. Heat Mass Transfer*, Vol. 46 No. 17, pp. 3179-88.

Forcada, M.L. and Mate, C.M. (1993), "Molecular layering during evaporation of ultra thin liquid films", *Nature*, Vol. 363 No. 6429, pp. 527-9.

Huisman, W.J., Peters, J.F., Zwanenburg, M.J., deVries, S.A., Derry, T.E., Abernathy, D. and vanderVeen, J.F. (1997), "Layering of a liquid metal in contact with a hard wall", *Nature*, Vol. 390 No. 6658, pp. 379-81.

Maruyama, S. (2000) "*Molecular dynamics method for microscale heat transfer*", in Minkowycz, W.J. and Sparrow, E.M. (Ed.), *Advances in numerical heat transfer*. Tayler & Francis, New York, pp. 189-226.

Maruyama, S. and Kimura, T. (1999a), "A molecular dynamics simulation of a bubble nucleation on solid surface", in *5th ASME-JSME Thermal Engineering Joint Conference*San Diego, USA, pp. 1-7.

Maruyama, S. and Kimura, T. (1999b), "A study on thermal resistance over a solid-liquid interface by the molecular dynamics method", *Thermal Science & Engineering*, Vol. 7 No. 1, pp. 63-8.

Maruyama, S., Kimura, T. and M.-C., L. (2002), "Molecular scale aspects of liquid contact on a solid surface", *Thermal Science and Engineering*, Vol. 10 No. 6, pp. 23-9.

Matsumoto, M. (1996), "Molecular dynamics simulation of interphase transport at liquid surfaces", *Fluid Phase Equilib.*, Vol. 125 No. 1-2, pp. 195-203.

Matsumoto, M. and Fujikawa, S. (1997), "Nonequilibrium vapor condensation: Molecular simulation and shock-tube experiment", *Microscale Thermophys. Eng.*, Vol. 1 No. 2, pp. 119-26.

Matsumoto, M., Yasuoka, K. and Kataoka, Y. (1994), "Evaporation and condensation at a liquid surface. Ii. Methanol", *J. Chem. Phys.*, Vol. 101 No. 9, pp. 7912-7.

Matsumoto, M., Yasuoka, K. and Kataoka, Y. (1995), "Molecular simulation of evaporation and condensation", *Fluid Phase Equilib.*, Vol. 104 pp. 431-9.

Meland, R. (2002), "Molecular exchange and its influence on the condensation coefficient", *J. Chem. Phys.*, Vol. 117 No. 15, pp. 7254-8.

Meland, R., Frezzotti, A., Ytrehus, T. and Hafskjold, B. (2004), "Nonequilibrium molecular-dynamics simulation of net evaporation and net condensation, and evaluation of the gas-kinetic boundary condition at the interphase", *Phys. Fluids*, Vol. 16 No. 2, pp. 223-43.

Nagayama, G. and Cheng, P. (2004), "Effects of interface wettability on microscale flow by molecular dynamics simulation", *Int. J. Heat Mass Transfer*, Vol. 47 No. 3, pp. 501-13.

Nagayama, G. and Tsuruta, T. (2003), "A general expression for the condensation coefficient based on transition state theory and molecular dynamics simulation", *J. Chem. Phys.*, Vol. 118 No. 3, pp.

1392-9.

Nagayama, G., Tsuruta, T. and Cheng, P. (2006), "Molecular dynamics simulation on bubble formation in a nanochannel", *Int. J. Heat Mass Transfer*, Vol. 49 No. 23-24, pp. 4437-43.

National Institute of Standards and Technology (NIST) (2005), "Thermophysical properties of fluid systems", available at: http://webbook.nist.gov/chemistry/fluid/ (accessed 15 January 2008)

Penner, S.S. (1952), "On the kinetics of evaporation", *J. Phys. Chem.*, Vol. 56 No. 4, pp. 475-9.

Poulikakos, D., Arcidiacono, S. and Maruyama, S. (2003), "Molecular dynamics simulation in nanoscale heat transfer: A review", *Microscale Thermophys. Eng.*, Vol. 7 No. 3, pp. 181-206.

Rapaport, D.C. (2004) *The art of molecular dynamics simulation*, Cambridge University Press, Cambridge.

Stoddard, S.D. and Ford, J. (1973), "Numerical experiment on the stochastic behavior of a lennard-jones gas system", *Phys. Rev. A*, Vol. 8 No. 3, pp. 1504-12.

Tsuruta, T. and Nagayama, G. (2002), "A molecular dynamics approach to interphase mass transfer between liquid and vapor", *Microscale Thermophys. Eng.*, Vol. 6 No. 4, pp. 267-85.

Tsuruta, T., Tanaka, H. and Masuoka, T. (1999), "Condensation/evaporation coefficient and velocity distributions at liquid-vapor interface", *Int. J. Heat Mass Transfer*, Vol. 42 No. 22, pp. 4107-16.

Wang, C.S., Chen, J.S., Shiomi, J. and Maruyama, S. (2007), "A study on the thermal resistance over solid-liquid-vapor interfaces in a finite-space by a molecular dynamics method", *Int. J. Therm. Sci.*, Vol. 46 pp. 1203-10.

Wegener, P.P. and Pouring, A.A. (1964), "Experiments on condensation of water vapor by homogeneous nucleation in nozzles", *Phys. Fluids*, Vol. 7 No. 3, pp. 352-61.

Xue, L., Keblinski, P., Phillpot, S.R., Choi, S.U.S. and Eastman, J.A. (2003), "Two regimes of thermal resistance at a liquid-solid interface", *J. Chem. Phys.*, Vol. 118 No. 1, pp. 337-9.

Xue, L., Keblinski, P., Phillpot, S.R., Choi, S.U.S. and Eastman, J.A. (2004), "Effect of liquid layering at the liquid-solid interface on thermal transport", *Int. J. Heat Mass Transfer*, Vol. 47 pp. 4277-84.

Yang, T.H. and Pan, C. (2005), "Molecular dynamics simulation of a thin water layer evaporation and evaporation coefficient", *Int. J. Heat Mass Transfer*, Vol. 48 No. 17, pp. 3516-26.

Yasuoka, K., Matsumoto, M. and Kataoka, Y. (1994), "Evaporation and condensation at a liquid surface. I. Argon", *J. Chem. Phys.*, Vol. 101 No. 9, pp. 7904-11.

Yi, P., Poulikakos, D., Walther, J. and Yadigaroglu, G. (2002), "Molecular dynamics simulation of vaporization of an ultra-thin liquid argon layer on a surface", *Int. J. Heat Mass Transfer*, Vol. 45 No. 10, pp. 2087-100.

Ziarani, A.S. and Mohamad, A.A. (2008), "Effect of wall roughness on the slip of fluid in a microchannel", *Nanoscale Microscale Thermophys. Eng.*, Vol. 12 No. 2, pp. 154-69.

Figure captions

Fig. 1 System configurations for smooth surface case (left) and rough surface case (right). Each contains fluid (argon, white) molecules and solid (platinum) atoms. The solid wall is comprised of real atoms (gray) and phantom atoms (dark). The insertion region is set at the top of the cuboid indicated by dash lines.

Fig. 2 Solid wall configuration of platinum atoms arranged in FCC (111) pattern (projection in the *y*-*z* plane). The solid wall is comprised of several layers of real atoms and two layers of phantom atoms with the lower layer fixed.

Fig. 3 Molecule insertion mechanics: (a) flow chart; (b) schematic.

Fig. 4 Velocity distribution of the vapor molecules in equilibrium period of S1~S3 cases. ΔN_v : the number of the vapor molecules with those velocities between v and $v+\Delta v$. N_0 : the number of vapor molecules in equilibrium period. Δv : increment of velocity. The downtriangle, circle and uptriangle symbols indicate the simulation data obtained from S1, S2 and S3 respectively. The solid lines indicate the Maxwellian distributions and $v_{m,i}$ ($i=1,2,3$) are the corresponding most probable velocities.

Fig. 5 Temporal variation of the density profile of S2 case ($t'=0\sim10\text{ns}$)

Fig. 6 Temporal variations of the temperature (upper panel) and the potential energy (middle panel) profiles of S2 case, and the enthalpy profile averaged over $t'=8\sim10\text{ns}$ (lower panel).

Fig. 7 Local radius distribution functions of S2 and S4~S8 cases corresponding to $t'=6\text{ns}$. The distribution functions are averaged in the volume between $z=-19.77\text{nm}$ and $z=-17.03\text{nm}$.

Fig. 8 Temporal variations of argon molecule numbers of S1~S8 cases.

Fig. 9 Initial velocity component distribution of the inserted vapor molecules in condensation period of S2 case. The solid line indicates the Gaussian distribution, from which the velocity components are sampled. The average value of the initial temperature of the inserted vapor molecules is 119.5K.

Fig. 10 Temporal values of q_l, q_sh/q_l and q_lh/q_l of S2 and S4~S8 cases corresponding to $t'=$ (a) 2ns, (b) 6ns and (c) 10ns. The circle symbols indicate q_l and the light gray and gray columns indicate q_sh/q_l and q_lh/q_l.

Fig. 11 Temporal variations of T_j and R of S2 and S4~S8 cases. The uptriangle, circle and downtriangle symbols indicate the values corresponding to $t'=2\text{ns}$, 6ns and 10ns, respectively.

Fig. 12 Two-dimensional profiles of density and temperature and systematic snapshots of (a)~(c): R7; (d)~(f): R3 and (g)~(i): R8.

Fig. 13 Density (upper panel) and temperature (lower panel) profiles in (a): *x-direction* and (b): *z-direction* of R3 case.

Fig. 14 Temporal variations of argon molecule numbers of R1~R8 cases.

Fig. 15 Temporal values of q_l, q_sh/q_l and q_lh/q_l of R1~R8 cases corresponding to $t'=$ (a) 2ns, (b) 6ns and (c) 10ns. The circle symbols indicate q_l and the light gray and gray columns indicate q_sh/q_l and q_lh/q_l.

Fig. 16 Temporal variations of T_j and R of R1~R8 cases. The uptriangle, circle and downtriangle symbols indicate the values corresponding to $t' = 2\text{ns}$, 6ns and 10ns, respectively.

Fig. 17 Comparison of increment ratios of $\overline{q}$ for different cases. ($\overline{q}$ are averaged over $t' = 2\text{ns}\sim10\text{ns}$ and all the increment ratios are defined taking the result of S2 case as the benchmark)

Figures

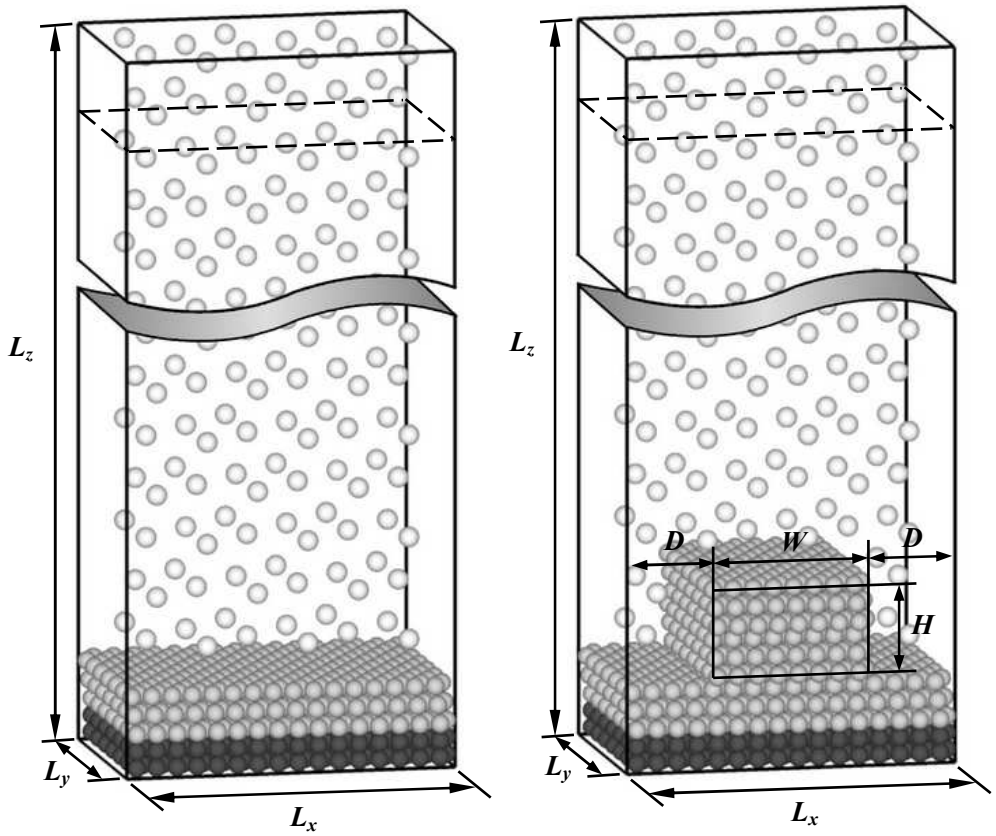

Fig. 1 System configurations for smooth surface case (left) and rough surface case (right). Each contains fluid (argon, white) molecules and solid (platinum) atoms. The solid wall is comprised of real atoms (gray) and phantom atoms (dark). The insertion region is set at the top of the cuboid indicated by dash lines.

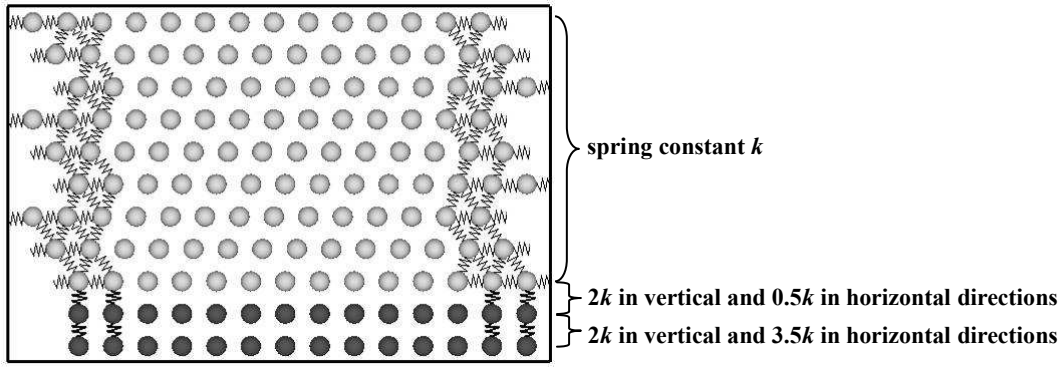

Fig. 2 Solid wall configuration of platinum atoms arranged in FCC (111) pattern (projection in the *y*-*z* plane). The solid wall is comprised of several layers of real atoms and two layers of phantom atoms with the lower layer fixed.

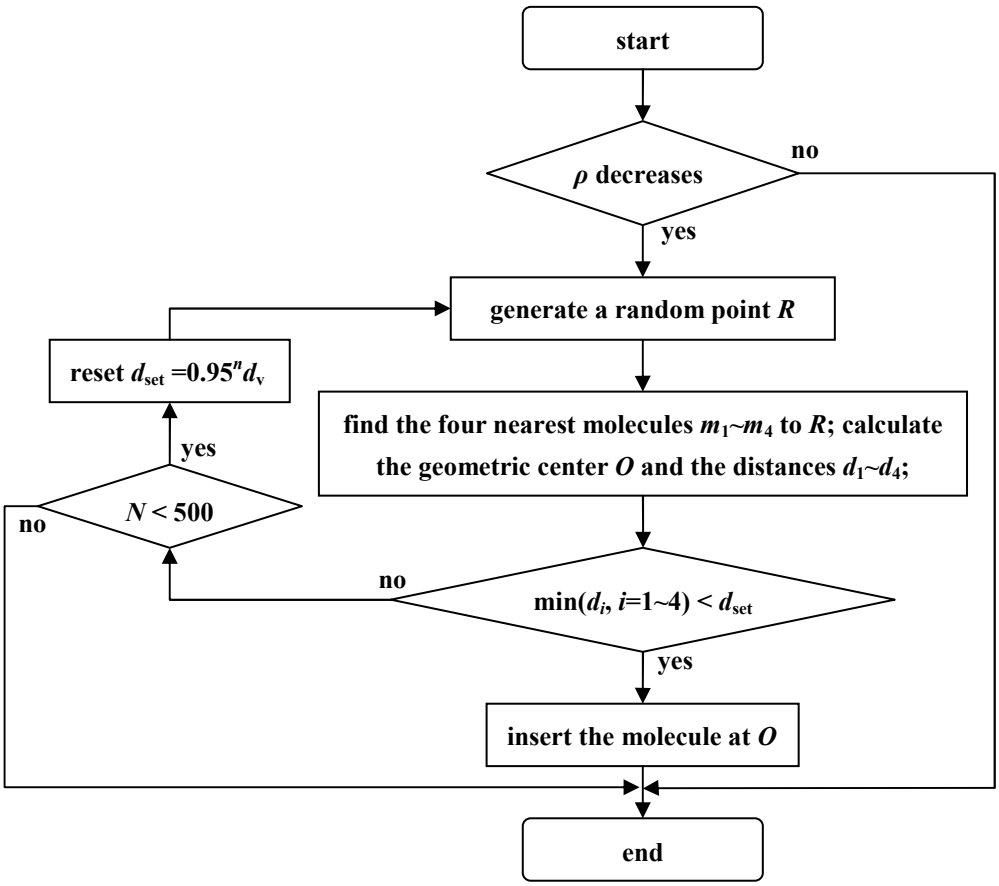

(a)

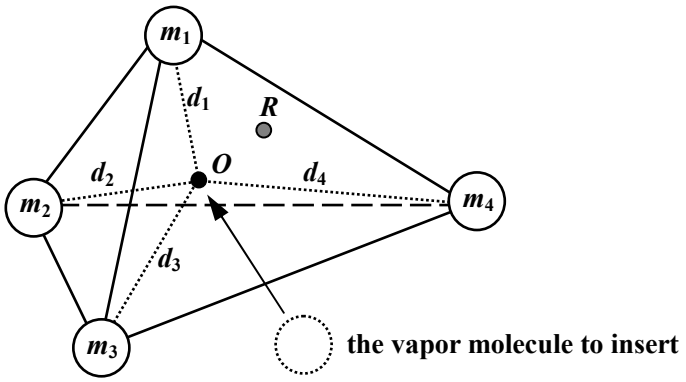

(b)

Fig. 3 Molecule insertion mechanics: (a) flow chart; (b) schematic.

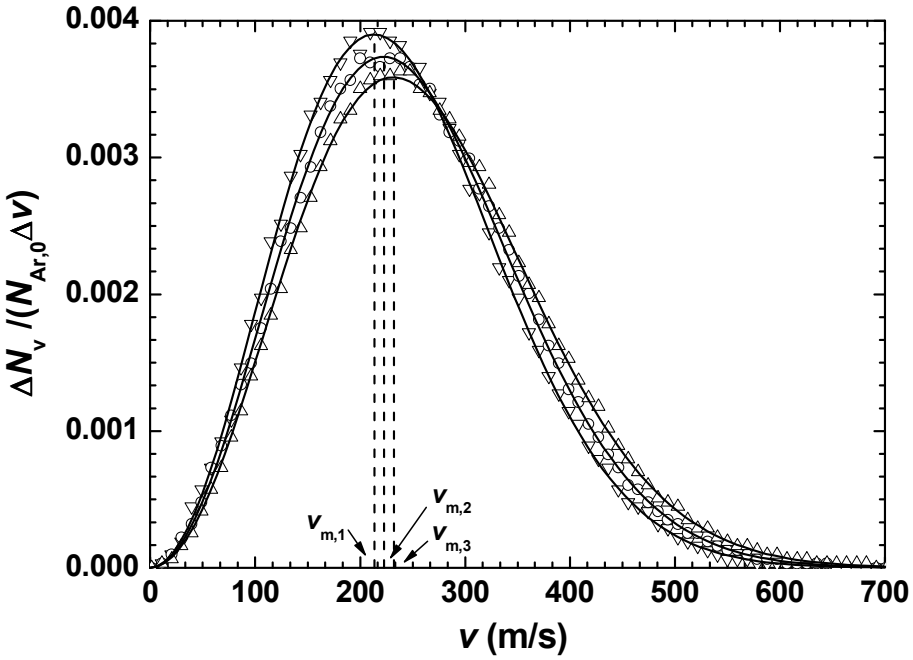

Fig. 4 Velocity distribution of the vapor molecules in equilibrium period of S1~S3 cases. ΔN_v : the number of the vapor molecules with those velocities between v and $v+\Delta v$. N_0 : the number of vapor molecules in equilibrium period. Δv : increment of velocity. The downtriangle, circle and uptriangle symbols indicate the simulation data obtained from S1, S2 and S3 respectively. The solid lines indicate the Maxwellian distributions and $v_{m,i}$ ($i = 1,2,3$) are the corresponding most probable velocities.

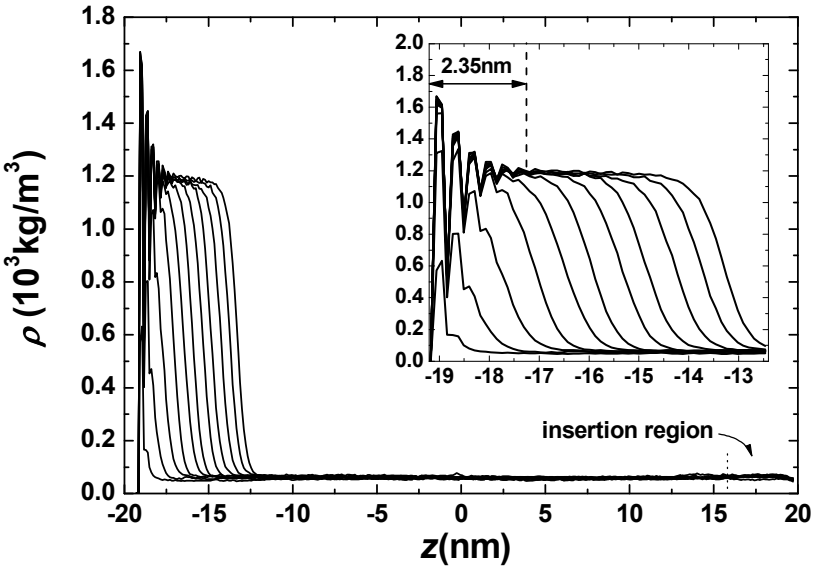

Fig. 5 Temporal variation of the density profile of S2 case ($t' = 0 \sim 10$ns)

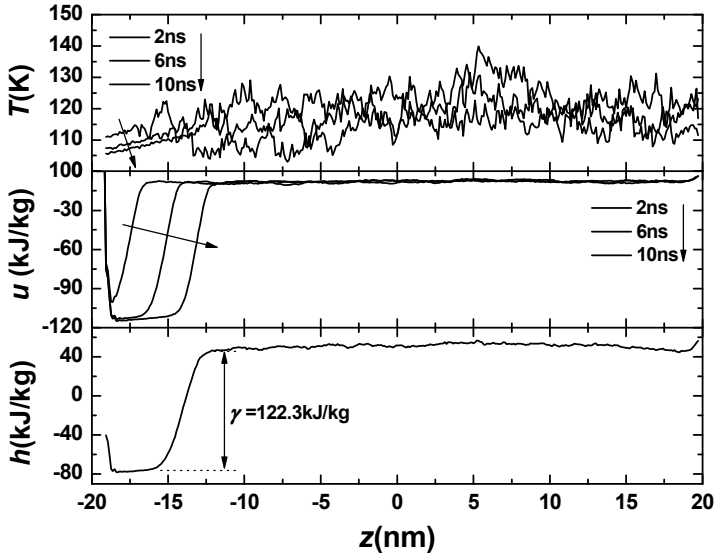

Fig. 6 Temporal variations of the temperature (upper panel) and the potential energy (middle panel) profiles of S2 case, and the enthalpy profile averaged over $t' = 8 \sim 10\text{ns}$ (lower panel).

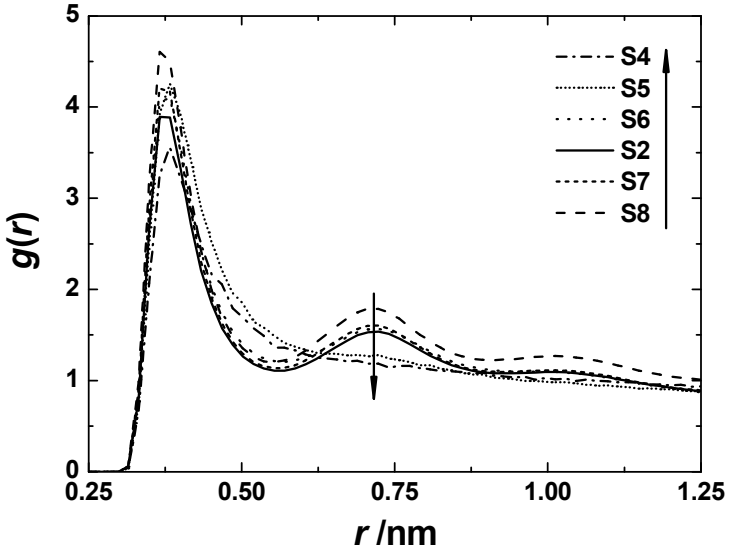

Fig. 7 Local radius distribution functions of S2 and S4~S8 cases corresponding to $t' = 6\text{ns}$. The distribution functions are averaged in the volume between $z = -19.77\text{nm}$ and $z = -17.03\text{nm}$.

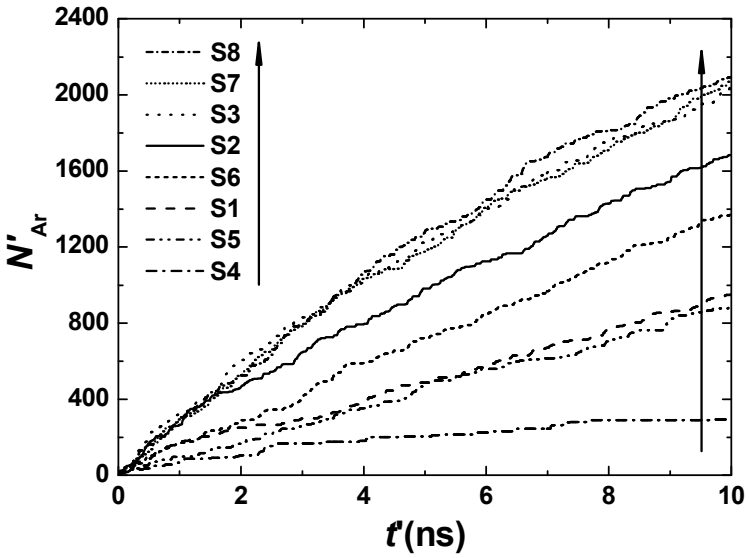

Fig. 8 Temporal variations of argon molecule numbers of S1~S8 cases.

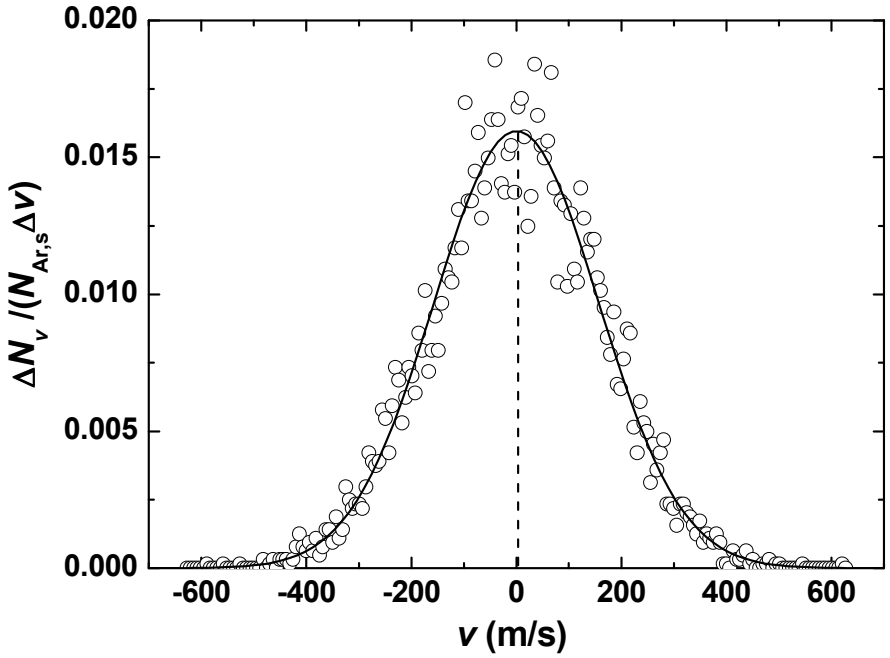

Fig. 9 Initial velocity component distribution of the inserted vapor molecules in condensation period of S2 case. The solid line indicates the Gaussian distribution, from which the velocity components are sampled. The average value of the initial temperature of the inserted vapor molecules is 119.5K.

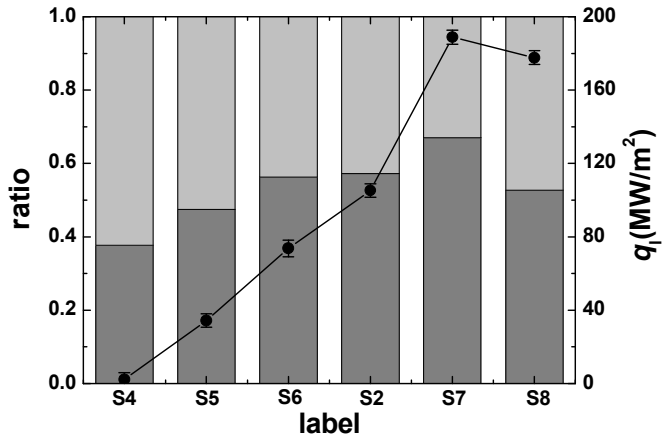

(a)

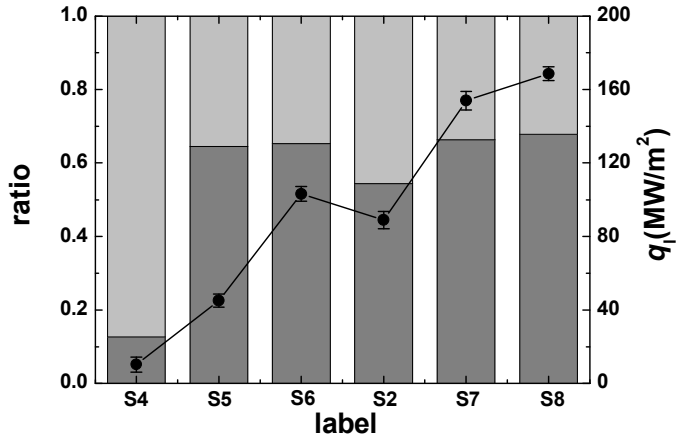

(b)

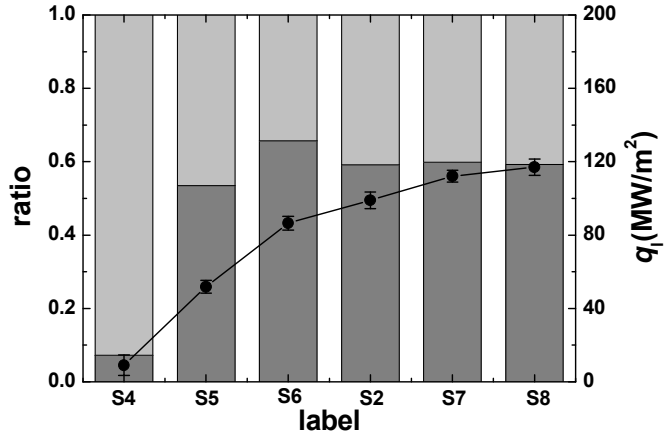

(c)

Fig. 10 Temporal values of q_l, q_{sh}/q_l and q_{lh}/q_l of S2 and S4~S8 cases corresponding to $t' =$ (a) 2ns, (b) 6ns and (c) 10ns. The circle symbols indicate q_l and the light gray and gray columns indicate q_{sh}/q_l and q_{lh}/q_l.

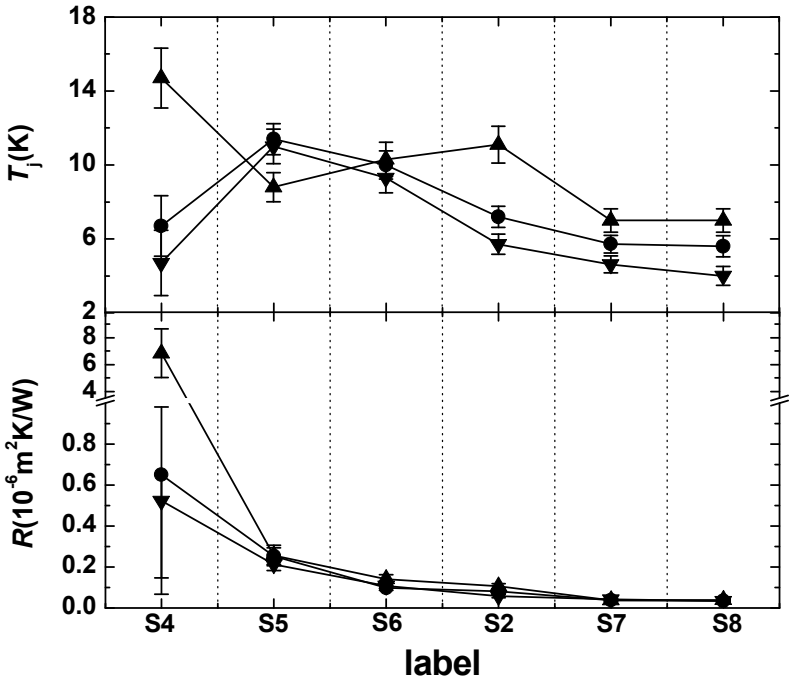

Fig. 11 Temporal variations of T_j and R of S2 and S4~S8 cases. The uptriangle, circle and downtriangle symbols indicate the values corresponding to $t' = 2\text{ns}$, 6ns and 10ns, respectively.

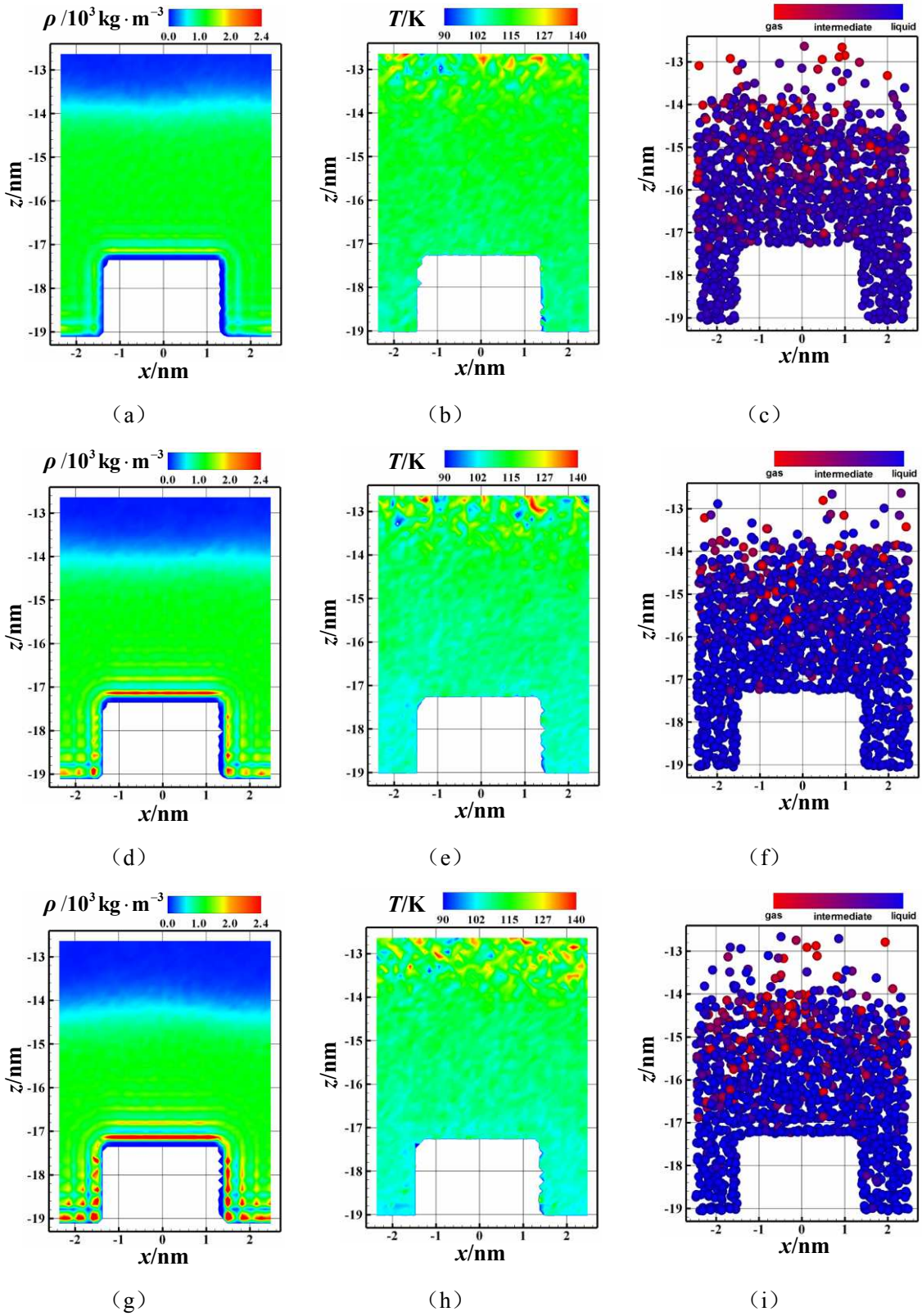

Fig. 12 Two-dimensional profiles of density and temperature and systematic snapshots of (a)~(c): R7; (d)~(f): R3 and (g)~(i): R8.

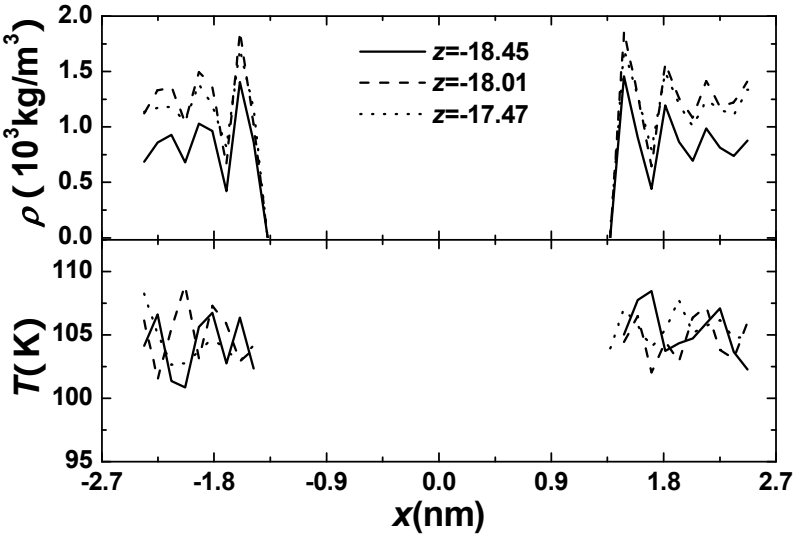

(a)

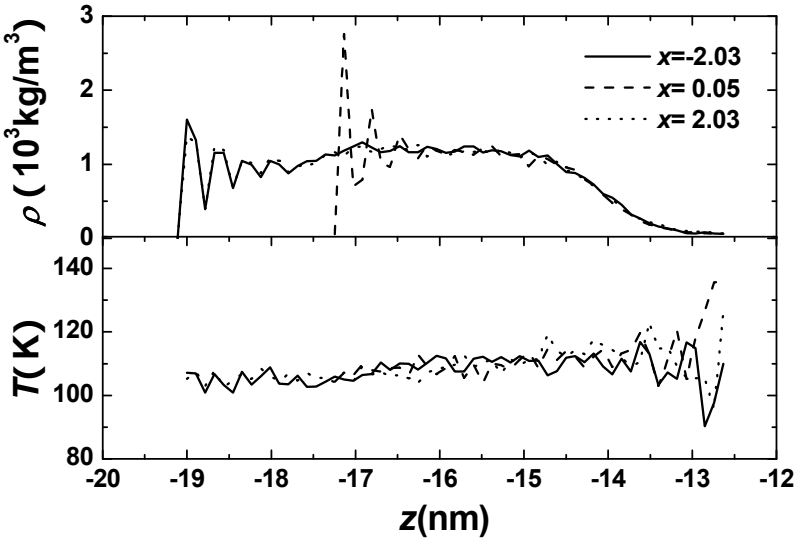

(b)

Fig. 13 Density (upper panel) and temperature (lower panel) profiles in (a): *x*-direction and (b): *z*-direction of R3 case.

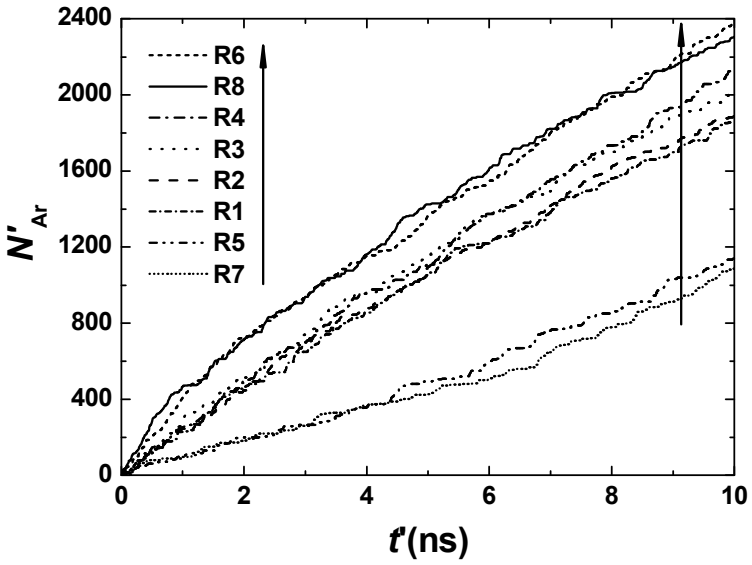

Fig. 14 Temporal variations of argon molecule numbers of R1~R8 cases.

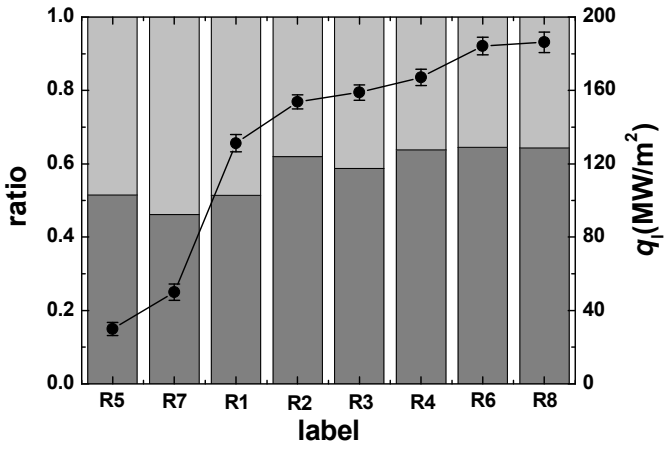

(a)

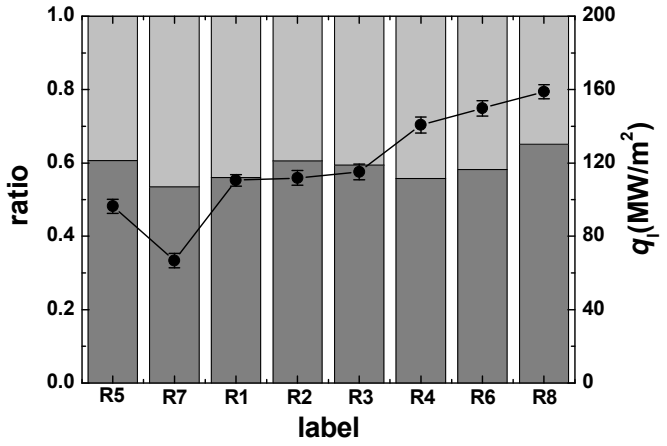

(b)

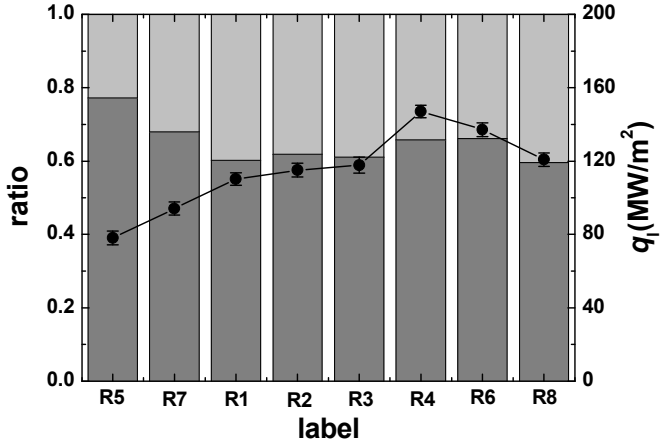

(c)

Fig. 15 Temporal values of q_{l}, $q_{\mathrm{sh}}/q_{\mathrm{l}}$ and $q_{\mathrm{lh}}/q_{\mathrm{l}}$ of R1~R8 cases corresponding to $t'=$ (a) 2ns, (b) 6ns and (c) 10ns. The circle symbols indicate q_{l} and the light gray and gray columns indicate $q_{\mathrm{sh}}/q_{\mathrm{l}}$ and $q_{\mathrm{lh}}/q_{\mathrm{l}}$.

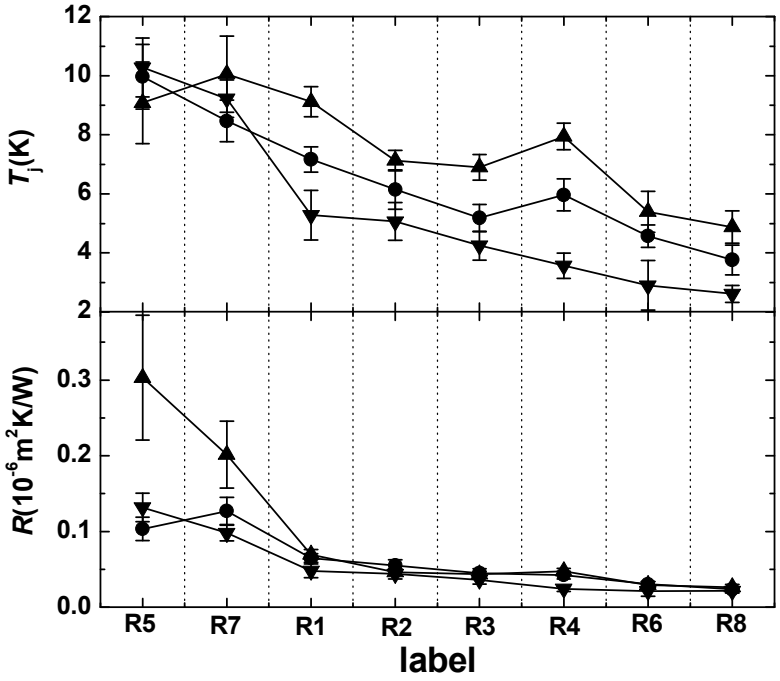

Fig. 16 Temporal variations of T_j and R of R1~R8 cases. The uptriangle, circle and downtriangle symbols indicate the values corresponding to $t' = 2\text{ns}$, 6ns and 10ns, respectively.

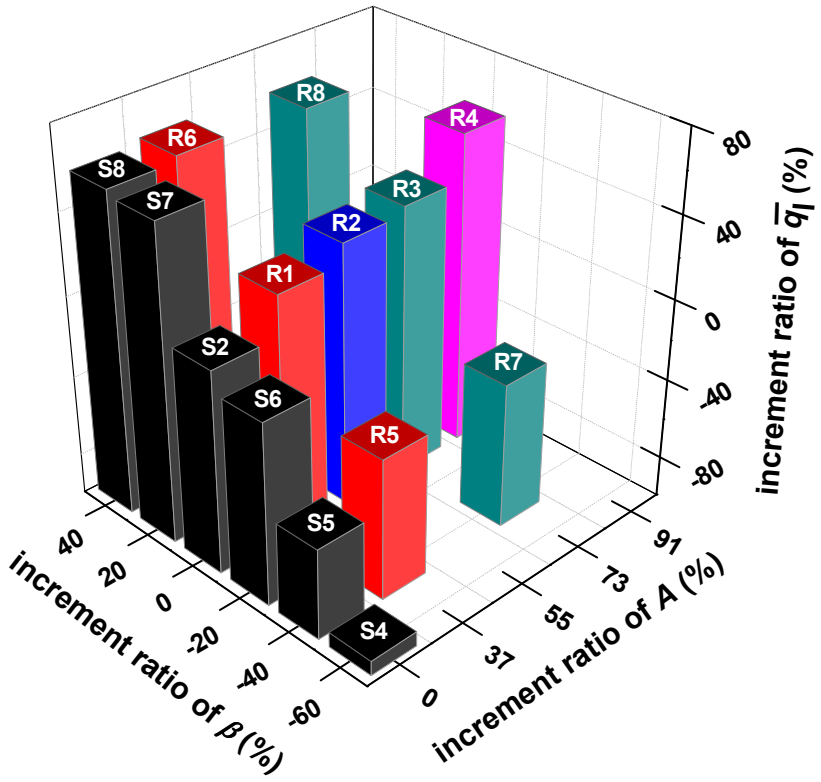

Fig. 17 Comparison of increment ratios of $\overline{q}$ for different cases. ($\overline{q}$ are averaged over $t' = 2\text{ns}\sim10\text{ns}$ and all the increment ratios are defined taking the result of S2 case as the benchmark)

Tables

Table 1 Simulation conditions

Smooth surface case					Rough surface case							
Label	β	L_x (nm)	L_y (nm)	L_z (nm)	Label	H (nm)	β	W (nm)	D (nm)	L_x (nm)	L_y (nm)	L_z (nm)
S1		6.014	4.009	48.11	R1	0.905						
S2	1.0	4.943	3.295	39.54	R2	1.357	1.0					
S3		4.097	2.731	32.78	R3	1.809						
S4	0.4				R4	2.262		2.632	1.156	4.943	3.295	39.54
S5	0.6				R5	0.905	0.6					
S6	0.8	4.943	3.295	39.54	R6		1.4					
S7	1.2				R7	1.809	0.6					
S8	1.4				R8		1.4					

Table 2 Simulation conditions and results for smooth surface cases*

Label	T_v (K)	T_w (K)	p_v (MPa)	$p_{v,e}$ (MPa)	ρ_v ($10^3 kg/m^3$)	$\rho_{v,e}$ ($10^3 kg/m^3$)	ρ_l ($10^3 kg/m^3$)	$\rho_{l,e}$ ($10^3 kg/m^3$)
S1	111.8	100.1	0.667	0.705	0.035	0.033	1.208	1.287
S2	122.4	100.1	1.254	1.246	0.060	0.061	1.196	1.261
S3	132.8	100.2	2.060	2.175	0.111	0.102	1.164	1.211

Label	$\dot{m}_c$ ($kg/s \cdot m^2$)	γ (kJ/kg)	γ_e (kJ/kg)	$\dot{q}_v$ (MW/m^2)	q_l (MW/m^2)	$\partial T/\partial z$ (K/nm)	λ_l ($W/m \cdot K$)	$\lambda_{l,e}$ ($W/m \cdot K$)	T_j (K)	k ($MW/m^2 \cdot K$)	R ($10^{-6} m^2 \cdot K/W$)
S1	259.4	130.8	137.6	35.23	69.2	0.732	0.095	0.104	3.30	5.91	0.048
S2	526.9	122.3	123.7	40.46	104.9	1.125	0.093	0.098	5.30	4.70	0.051
S3	881.2	96.6	103.1	45.12	130.2	1.433	0.091	0.090	7.01	3.99	0.054

* $p_{v,e}$, $\rho_{v,e}$, $p_{l,e}$, γ_e and $\lambda_{l,e}$ are experimental values (NIST, 2005).